Nigerian Journal of Applied Physics (NJAP)
ISSN Print: 3115-5871
ISSN Online: 3115-588X
DOI: https://doi.org/10.62292/njap-v2i1-2026-65
Volume 2(1), March 2026

Structural and Electrochemical Properties of Graphene Oxide Nanoparticles Synthesized via Modified Hummers Method for Energy Storage Electrodes

***[1,2]Okorie Okike, [2]Buba Ardo Dahiru Abdul and [2]Umar Medina**

[1]Department of Theoretical Physics, National Mathematical Centre, FCT Abuja, Nigeria.
[2]Department of Physics, Faculty of Science, University of Abuja, FCT Abuja, Nigeria.

[*]Corresponding author's email: okike_isu@yahoo.com

ABSTRACT

Graphene Oxide (GO) nanoparticles of high quality were synthesized using the improved modified Hummers method. Their morphological and structural properties were thoroughly investigated. SEM analysis revealed flake-like, irregular layered fragments typical of GO sheets, with a rough and uneven surface texture resulting from exfoliation and oxidation. XRD analysis showed a distinct peak at ~9.2°, corresponding to the (001) diffraction plane of GO, indicative of increased interlayer spacing due to oxygen functional groups and intercalated water molecules formed during graphite oxidation. Using the Williamson–Hall equation, the particle size was calculated to be 10.96 nm with a strain value of 0.1767. This indicates that the graphene oxide nanoparticles are extremely small and exhibit significant lattice strain, suggesting a high density of defects and enhanced chemical activity — conditions that are particularly favorable for forming composites. BET analysis indicated a specific surface area of 255.66 m^2/g and a pore size distribution of 2.137 nm. FT-IR spectra confirmed the presence of oxygen-containing functional groups (hydroxyl, epoxy, and carboxyl), which impart hydrophilicity and chemical reactivity, making GO suitable for composites, membranes, and biomedical applications. Electrochemical evaluation of the synthesized graphene oxide revealed promising performance, delivering an energy density of 6.54 Wh/kg and a power density of 40.16 kW/kg. These values is an indication that the material as more suitable for supercapacitor applications than for conventional batteries. EIS analysis further revealed an electrochemical series resistance (ESR) of 13.8 Ω and a charge transfer resistance (Rct) of 107.38 Ω, underscoring the material's potential for energy storage applications.

Keywords:
Energy Storage,
Graphene Oxide,
BET Surface Analysis,
Supercapacitors,
Williamson -Hall equation.

INTRODUCTION

The ever – growing demand for portable energy storage devices for application in different fields got a boost since the discovery of Graphene in 2004 (Novoselov K. , et al., 2004) providing an alternative material for energy storage systems other than the traditional energy solution from fossil fuel (Hossain, et al., 2023) thereby saving the environment from pollution. These energy storage systems have been gaining serious attention in the recent years and are regarded as electrochemical energy storage devices (Vessally, Rzayev, Niyazova, Aggarwal, & Rahimova, 2024).

The electrochemical energy storage technologies are fuel cells which is regarded as open system because the cathodes are responsible for carrying out charge transfer within the system, and a closed system which are batteries and supercapacitors where charge interaction involves the mass of the active material in the electrodes (Fagiolari, et al., 2022; Mujib, Ribot, Gervais, & Singh, 2021). Batteries primarily store energy through electrode reactions, known as faradaic processes, though depending on the system, non-faradaic contributions may also occur (Vessally, Rzayev, Niyazova, Aggarwal, & Rahimova, 2024). In contrast, supercapacitors are categorized by their energy storage mechanisms: electrochemical double-layer capacitors (EDLCs), pseudocapacitors, and hybrid types that combine both EDLC and pseudocapacitive behavior (Vangari, Pryor, & Jiang, 2013).

Graphene oxide (GO), a two-dimensional carbon-based nanomaterial, features a distinctive layered architecture functionalized with oxygen-containing groups such as

hydroxyl, epoxy, and carboxyl moieties. These functional groups, located on both surfaces and at the sheet edges, impart hydrophilicity and chemical tunability, setting GO apart from pristine graphene (Zhan, Xu, Lin, Haijie, & He, 2025; Shin, et al., 2017; Thakur, et al., 2026). The distinctive physiochemical properties of GO are advantageous for its application in several fields like healthcare and sensing (Baruah, et al., 2024), environmental remediation (Goyat, Saharan, Singh, Umar, & Akbar, 2022), water treatment (Pan, et al., 2018), energy conversion and storage as well as catalysis (Thakur, et al., 2026; Ghafuri, et al., 2025).

The synthesis method adopted in the production of graphene electrodes is of paramount importance because a lot of studies show that it has a lot to do with their properties, including their electrical conductivity, surface area and morphology, defect density, and overall performance, with factors like the chosen precursor, chemical treatment, temperature, and reaction time all playing a crucial role in determining the final quality of the graphene electrode.

Offeman introduced what is now recognized as the Hummers method, a relatively safe approach for preparing graphitic oxide from graphite using an essentially anhydrous mixture of sulfuric acid, sodium nitrate, and potassium permanganate (Hummers & Offeman, 1958).

Broadly, graphene synthesis techniques can be categorized into two principal groups: top–down (destructive) methods and bottom–up (constructive) methods. Top–down approaches typically involve the reduction or exfoliation of powdered graphite (Kumar, et al., 2021). Prominent techniques include mechanical exfoliation, micromechanical cleavage, liquid-phase exfoliation, plasma etching, electrochemical exfoliation, laser ablation, ball milling, sonication, and chemical oxidation–reduction (Mbayachi, et al., 2021). The Nobel Prize–winning mechanical exfoliation method developed by Novoselov and colleagues exemplifies a top–down synthesis route. In this process, household adhesive tape was employed to mechanically peel single-layer graphene (SLG) sheets, with lateral dimensions on the micrometer scale, from highly oriented pyrolytic graphite (HOPG) (Novoselov K. S., et al., 2004). Despite its historical significance, the method suffers from low yield and limited scalability, producing only small surface areas of SLG, thereby restricting its suitability for large-scale production (Liu, Chai, Mohamed, & Hashim, 2014; Ye & Tour, 2019) in addition, only a tiny surface area of the single-layer graphene (SLG) film could be produced (Lee, et al., 2017).

Chemical exfoliation is widely recognized as the most popular, efficient, and cost-effective top–down synthesis route for graphene when compared with other established techniques. The process typically begins with the oxidation of graphite into graphite oxide, followed by its reduction into graphene through chemical, thermal, or electrochemical methods. Various oxidation strategies have been employed, often involving concentrated acids and strong oxidizing agents (Brodie, 1859; Staudenmaier, 1899; Hummers & Offeman, 1958). During exfoliation, graphite layers are separated via redox reactions, which serve to weaken van der Waals forces by increasing interlayer spacing between flakes (Abakumov, Bychko, & Trypolskii, 2021). Although, it is a highly efficient synthesis technique; however, extremely hazardous oxidizing agents such as potassium permanganate ($KMnO_4$) are traditionally used in this technique, raising environmental and safety concerns.

Consequently, attention has now been shifted towards the use of less harmful chemicals as oxidizing agents, and several studies have been conducted using chemical exfoliation with less harmful chemicals utilized as oxidizing agents. Some researchers have been using different environmentally friendly substances (termed green reducers) to produce functional graphene sheets (Aunkor, Mahbubul, Saidurb, & Metselaar, 2016).

In contrast, bottom–up synthesis utilizes hydrocarbon precursors—both gaseous and liquid—which decompose to form graphene layers with a hexagonal lattice (Yoon & Dong, 2019). Prominent bottom–up techniques include chemical vapor deposition (CVD) (Sun, et al., 2021), thermal pyrolysis (Thangaraj, et al., 2023), epitaxial growth (Yazdi, Iakimov, & Yakimova, 2016), laser-assisted synthesis (AtiafK.Jeryo & Abbas, 2020), and organic synthesis routes (Abbas, et al., 2022).

In this study, the synthesis of graphene oxide (GO) follows the method developed by Hummers and Offeman, selected for three key advantages: (i) relatively short reaction times, typically completed within a few hours; (ii) substitution of potassium chlorate with potassium permanganate, ensuring safer reaction conditions; (iii) the use of sodium nitrate, which effectively eliminates acid mist formation (Hummers & Offeman, 1958); and above all (iv) it doesn't require sophisticated machinery that is out of reach to the developing countries and also the materials are readily available and relatively cheap. Indeed, an established safe, reproducible protocol from graphite powder, and controlled oxidation level to achieve GO nanoparticle with high specific surface area (SSA) which will provide more active sites for charge storage, mesoporous channels for fast ion transport and possibly for composite formation.

MATERIALS AND METHODS

The reagents and solvents used in this work are; Graphite powder (Carbon – 98%, Fe – 0.4%, Sulphur – 0.1%, Ash content – 0.7%, Phosphorous – Traces), Potassium permanganate ($KMnO_4$), Sodium nitrate (Na_2NO_3), Hydrogen Peroxide (H_2O_2), sulphuric acid (H_2SO_4, 98%), Hydrochloric acid (HCl) and Distilled water which were of analytical grade and purchased from Molychem India.

All the chemicals were used as received without further purification.

Graphene oxide (GO) was synthesized via the modified Hummers method, which was earlier reported (Mahdi, Javanbakht, & Shahrokhian, 2024) 4 grams of graphite powder and 4 grams of sodium nitrate ($NaNO_3$) in the ratio of 4:4 were mixed in 150 ml of concentrated sulphuric acid (H_2SO_4) in a beaker and placed in an ice bath and sonicated for about 30 minutes to ensure complete dissolution using EINS SCI Sonicator Model E-uc6-HD-D after which 20 grams of Potassium permanganate ($KMnO_4$) was slowly added to the mixture to enhance the oxidation process maintaining the temperature between 15°C - 20°C so as to control the exothermic reaction in the system. The solution was stirred at an elevated temperature within the range of 35–50 °C for about three hours before diluting it with deionized water. In order to dilute and quench the reaction, deionized water was carefully added to the solution while stirring although at this point the temperature suddenly rose to about 80°C. 30 ml of 35% Hydrogen peroxide (H_2O_2) was added to terminate the reaction and remove any remaining Potassium permanganate. It was centrifuged using Cole model 0406-2 centrifuge set on 3000rpm for 15 minutes, followed by washing the synthesized graphite oxide with 10% Hydrochloric acid and then with deionized water to remove any residual acids and salts. The graphite oxide was collected as powder, dried at room temperature for 48hrs to bring the final product to graphene oxide (GO).

RESULTS AND DISCUSSION

A number of physical/structural characterization technique were deployed to determine the morphology, composition and characteristics of the composite. The fundamental analysis for qualitative, quantitative and clarification of properties and structure of the composite is to be carried out using X-ray diffraction. Therefore, XRD in conjunction with some other techniques will give a full understanding of the physical/structural characteristics of the composite (Ali, Chiang, & Santos, 2022). XRD technique has the advantage of utilizing small amount of sample for the testing and also is non – destructive. Whereas Electrochemical characterization involves techniques like Cyclic Voltammetry (CV), and Electrochemical Impedance Spectroscopy (EIS) for determining the specific capacitance, power/energy density, equivalent series resistance (ESR) as well as charge kinetic behaviour.

XRD Analysis

X-ray diffraction (XRD) analysis was carried out using a Rigaku Miniflex-II diffractometer operated at 40 kV and 15 mA with CuKα radiation (λ = 1.5406 Å). The measurements were performed with a scanning speed of 20° per minute and a step size of 0.02°. The diffraction patterns were recorded over a 2θ range of 20° to 70°. Williamson–Hall (W-H) Equation (4) linked the peak broadening to micro strain as well as the crystallite size (Speakman; Williamson & Hall, 1953) hence separates size and strain contributions to peak broadening, offering a more in-depth analysis to crystallite size than what was believed. it therefore means that;

$$Total\ broadening\ (\beta_\tau) = broadening\ due\ to\ crystallite\ size\ (\beta_c) + broadening\ due\ to\ micro\ strain(\beta_\varepsilon)$$

$$i.e$$

$$(\beta_\tau) = (\beta_D) + (\beta_\varepsilon) \quad (1)$$

Also, the broadening due to micro strain is given as

$$\beta_\varepsilon = 4\varepsilon \tan\theta_D \quad (2)$$

Where:

β_ε= broadening due to strain, ε = the strain, θ = peak position in radians

From Braggs equation, and Scherrer's Equation, (1) now becomes

$$\beta_\tau = \frac{k\lambda}{Dcos\theta} + 4\varepsilon \tan\theta \quad (3)$$

Linearizing equation (3) will give Williamson–Hall (W-H) equation as shown in (4);

$$\beta_\tau cos\theta = \frac{k\lambda}{D} + 4\varepsilon \sin\theta \quad (4)$$

Where;

D = average crystallite size, K = shape factor (~0.9), λ = X-ray wavelength (0.15406)

β = full width at half maximum (FWHM) of the peak (in radians), θ = Bragg angle

ε = micro strain

Equation (4) is now a straight-line equation where we can extract the micro strain as the slope while the crystallite size will be calculated from the intercept.

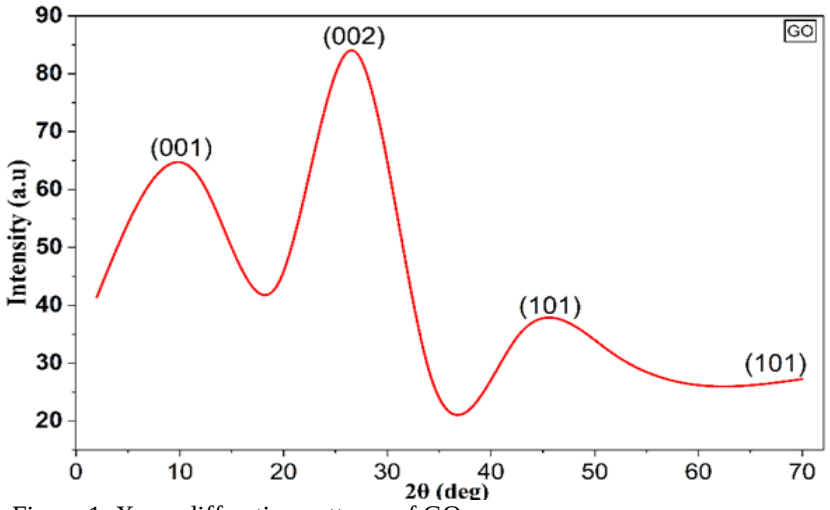

Figure 1: X-ray diffraction patterns of GO

Figure 1 shows the XRD diffractogram of the synthesized graphene Oxide. The (001) peak at ~9.2° is characteristic of GO due to increased interlayer spacing from oxygen functional groups and water molecules arising from the oxidation of the graphite powder and is referenced in the JCPDS card number 01-0646. This is true from our result that the interlayer spacing of the pristine graphite is 0.33nm or 3.3Å and the interlayer spacing of the GO is 0.959 nm or 9.59Å from our result shown table 1, which is also in agreement with the experimental results found in literatures (Krishnamoorthy, Veerapandian, Yun, & Kim, 2013). This means that the peak broadening effect is due to the lattice distortion which is as a result of oxidation. The peak at ~26.8° may indicate partial reduction or graphitic domains which may be as a result of method of drying which tends to restoring the sp^2 carbon networks because the drying methods usually affects the structure and this is in agreement with the findings of some other researchers (Huang, Park, & Huang, 2022). Higher-angle peaks (44.6° and 66.1°) though not primary identifiers for GO but can provide insight into its structural evolution. While some opined that these peaks correspond to inn-plane atomic arrangements typical of graphite domains which could arise as a result of partial reduction, multilayered, or graphitic domains (Hansora, Shimpi, & Mishra, 2015) So that they correspond to in-plane atomic arrangements and are typical in graphite-like structures characteristic of GO shown and summarized in table 1 with the interplanar spacing and from W– H plot the crystallite size and the micro strain were determined to be 10.96 nm and strain of 0.1767 respectively which implies that strain is the major contributor to the peak broadening. Some researchers reported W-H crystallite sizes for GO in the range of 8–12 nm, with strain values around 0.15–0.18, which align closely with our GO sample (Narayana & Jammalamadaka, 2016).

FT-IR Analysis

Table 1: Interlayer spacing and the Miller Indices of GO Sample

2θ (°)	θ (°)	FWHM (°)	d-spacing (nm)	Likely (hkl)
9.21584	4.60792	18.27317	0.959	(001) — GO interlayer spacing
26.82357	13.41179	10.30205	0.332	(002) — graphitic planes
44.56677	22.28339	14.60077	0.203	(101) — in-plane C–C spacing
66.08784	33.04392	44.54457	0.141	(110) — higher-order reflection

The Fourier-transform infrared (FTIR) spectrum of graphene oxide (GO) was recorded using a PerkinElmer Spectrum IR (Version 10.7.2), as presented in Fig. 2. The observed absorption peaks confirm the successful formation of GO. The principal bands and their corresponding assignments are as follows: a broad peak at 3382 cm^{-1} attributed to O–H stretching vibrations of hydroxyl groups on GO, (2110 cm^{-1}) may be attributed to residual CO_2 or weak alkyne-like vibrations, sometimes seen in GO spectra. (1621 cm^{-1}) C=C stretching from aromatic domains or C=O stretching from carboxyl/amide groups. (1043 cm^{-1}) C–O stretching, typical of epoxy or alkoxy groups in GO and (883 & 665 cm^{-1}) Out-of-plane C–H bending, linked to aromatic ring vibrations. These observations were in agreement with the results in other recent research works. Our spectrum confirms the presence of oxygen-containing functional groups (hydroxyl, epoxy, carboxyl) that are characteristic of GO. These groups are responsible for GO's hydrophilicity and reactivity, making it useful in composites, membranes, and biomedical applications (Andre, 2019; Brusko, Khannanov, Rakhmatullin, & Dimiev, 2024; Surekha, Krishnaiah, Ravi, & Suvarna, 2020).

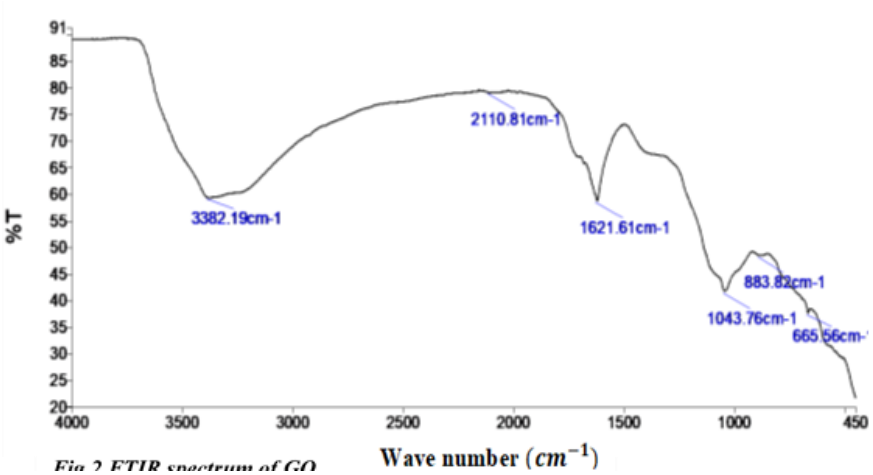

Figure 2: FTIR spectrum of GO

SEM Analysis

Nanos Semplor scanning electron microscope was used to check the morphology of GO Nanoparticle and is shown in figure 3. The images of the GO show flake – like irregular, layered fragments typical of GO sheets with rough uneven surface texture which may be as a result of exfoliation and oxidation process.

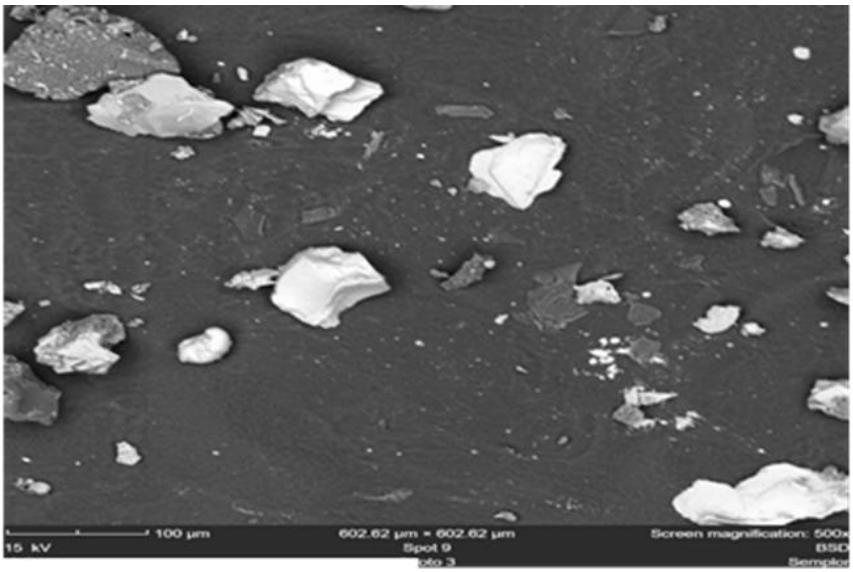

Figure 3: SEM Micrograph of GO

Energy Dispersion X-ray Spectroscopy (EDX) Analysis

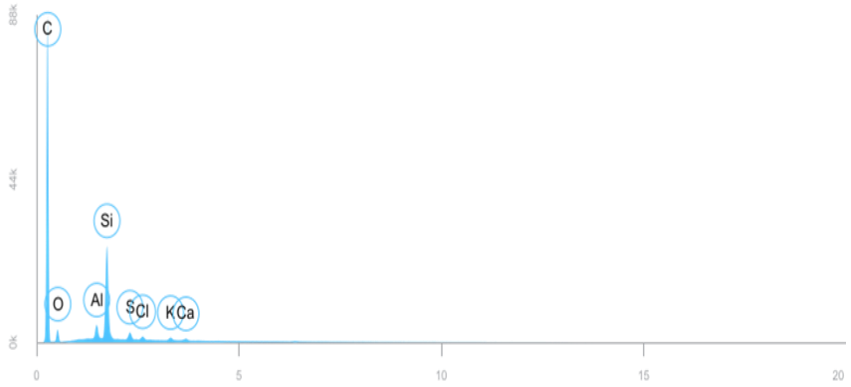

Figure 4: EDX Spectroscopy of GO

Nanos Semplor scanning electron microscope which is an instrument designed for both imaging and elemental analysis was used for the elemental analysis. The elemental composition is presented in figure 4 and summarized in table 2. The result confirms the dominant element to be carbon with percentage weight composition of 73.8% and percentage atomic composition to be 81.0% followed by oxygen that has percentage weight composition of 19.3% and percentage atomic composition of 15.9% and impurities $\approx \leq 5$ and it is in conformity with established standards (Nováček, et al., 2017; Mehmood, Shah, Omer, Idrees, & Saeed, 2024).

Surface Area and Pore Size Assessment

Table 2: Percentage Elemental Composition of Synthesized GO

Element	C	0	Si	Al	S	K	Cl	Ca
Weight%	73.8	19.3	4.8	0.7	0.5	0.3	0.3	0.2
Atom%	81.0	15.9	2.3	0.4	0.2	0.1	0.1	0.1

The Brunauer–Emmett–Teller (BET) specific surface area was determined from low-temperature nitrogen adsorption isotherms measured using a Nova Station a (Quantachrome Instruments, Version 11.0, Miami, FL, USA). Pore diameter, expressed in nanometers, was evaluated using the Barrett–Joyner–Halenda (BJH) method with the same instrument. The linearized form of BET equation (Schlumberger & Thommes, 2021; Brunauer, Emmett, & Teller, 1938) is given in (5) was used to extract the monolayer adsorbed gas volume which was applied to calculate the specific surface area (SSA).

$$\frac{P}{V(P_o-P)} = \frac{1}{V_m C} + \frac{C-1}{V_m C}.\frac{P}{P_o} \quad (5)$$

Where:

P = equilibrium pressure of adsorbate, P_o = saturation pressure, V = volume of gas adsorbed

V_m = monolayer capacity (volume of gas adsorbed at STP, in cm³/g)

C = BET constant (related to adsorption energy)

From (5) BET constant could be extracted through linear – regression which gives V_m and "C" as;

$$V_m = \frac{1}{slope+intercept}$$

And $C = 1 + \frac{\text{slope}}{\text{intercept}}$

And hence, the specific surface area is determined which is given by (6).

$$S_{BET} = \frac{V_m N_A \sigma}{v} \quad (6)$$

Where;

N_A= Avogadro's number (6.022×10^{23}), σ= molecular cross-sectional area of adsorbate (in m²)

v = molar volume of gas at (STP) 22,414 (cm³/mol) (Sing, et al., 1985; Brame & Griggs, 2016).

The BET linear plot (Figure 5) was constructed by plotting $1/\left[V\left(\left(\frac{P_o}{P}\right)-1\right)\right]$ against $\left(\frac{P}{P_0}\right)$. The linear region between 0.05–0.30 relative pressure was selected for fitting, and the result as calculated from the plot show that the monolayer capacity V_m was$0.05874 cm^3 g^{-1}$, the BET surface area is$255.66\ m^2 g^{-1}$. The BET constant (C) was also recorded as 5.889, indicating strong adsorbate–adsorbent interactions, also the linear regression(R^2) constant was 0.9738. The pore size was found to be 2.137 nm showing that it is a good mesoporous material for energy storage system. A high specific surface area combined with well-defined porosity is essential for maximizing the capacitance of supercapacitors. The results obtained in this study confirm that these properties

are present in the synthesized material, thereby providing a clear indication of its promising performance in energy storage applications.

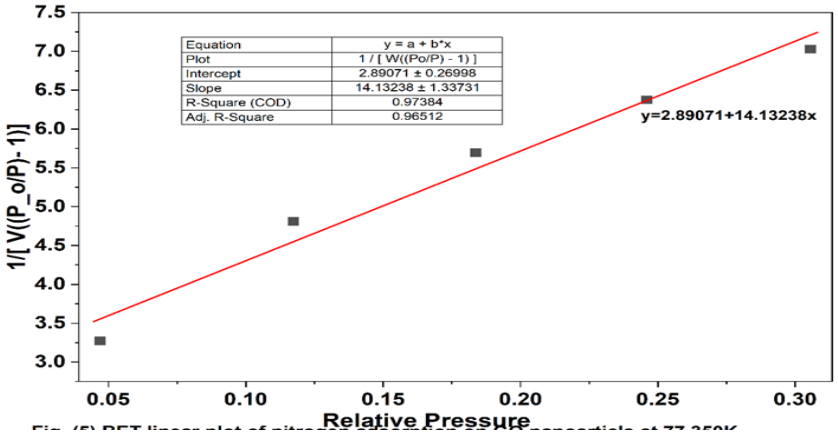

Figure 5: BET Linear plot of nitrogen absorption on GO nanoarticls at 77.350K

Electrochemical Analysis

The electrochemical properties of graphene oxide (GO) were investigated using cyclic voltammetry (CV) and electrochemical impedance spectroscopy (EIS). CV measurements were performed with a BioLogic SP-200 potentiostat employing a saturated calomel electrode (SCE) as the reference electrode. The potential was cycled between –2.50 V and +2.50 V at a scan rate of 50 mV s^{-1} over 10 successive cycles. The resulting voltammogram exhibited an anodic peak at +1.19 V and a cathodic peak at –0.30 V, corresponding to a peak separation (ΔEp) of approximately 1.49 V. The mass of the active material used was 0.001 g. EIS analysis was conducted using the same potentiostat over a frequency range of 100 kHz to 0.1 Hz with a 10 mV AC perturbation. The cyclic voltammograms obtained from CV are presented in Fig. 6, the CV curve does not appear perfectly rectangular rather distorted or non-ideal due to the presence of oxygen-containing functional groups, defects, and limited electrical conductivity. Rectangular CV curves are characteristic of ideal capacitive behavior (like in pure graphene or activated carbon), but GO's redox-active sites are what introduced peaks and deviations (Politano, Burza, & Versace, 2023; Brownson, Lacombe, Go´mez-Mingotb, & Banks, 2012). while the Nyquist plot used to extract electrochemical series resistance (ESR) and charge transfer resistance (Rct) values is shown in Fig. 7.From (5) the specific capacitance (C_{sp}) was calculated (Gharbi, Tran, Tribollet, Turmine, & Vivier, 2020; Libber, Gariya, & Kumar, 2025).

$$C_{sp} = \frac{S}{2mK\Delta V} \quad (7)$$

Where

C_{sp} = specific capacitance (Fg^{-1}), S = integral charge surface area of the CV curve in (mA.V),

m = mass of the electrode material in (g), V = value of the electrode potential in (V).

k = scan rate in (mV/s) and 2 is an indication of the forward and reverse sweeps.

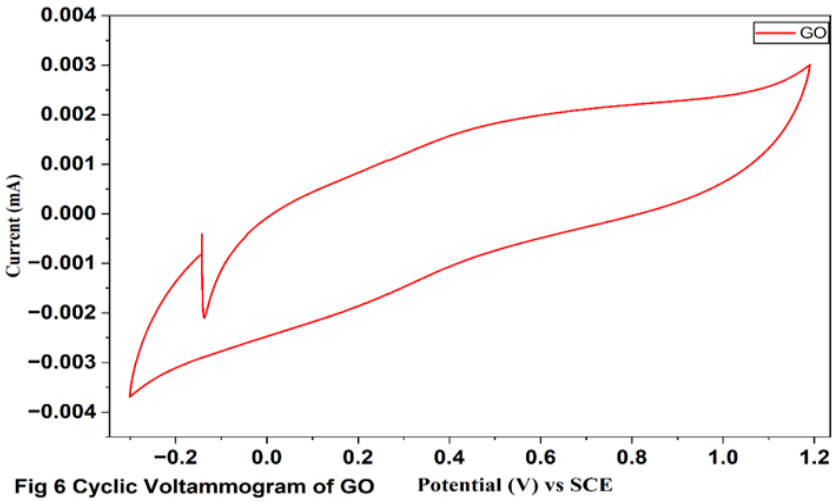

Fig 6 Cyclic Voltammogram of GO

The specific capacitance values were further utilized to calculate the energy density (E_d) in watt-hours per kilogram (Wh/kg) and the power density (P_d) in watts per kilogram (W/kg). These parameters were evaluated using equations (6) and (7), respectively. (Huld, et al., 2023).

$$E_d = \frac{1}{2} C_{sp} (\Delta V)^2 \quad (8)$$

$$P_d = \frac{V^2}{4 \times ESR \times m} \quad (9)$$

Where, ESR is the equivalent series resistance of the cell

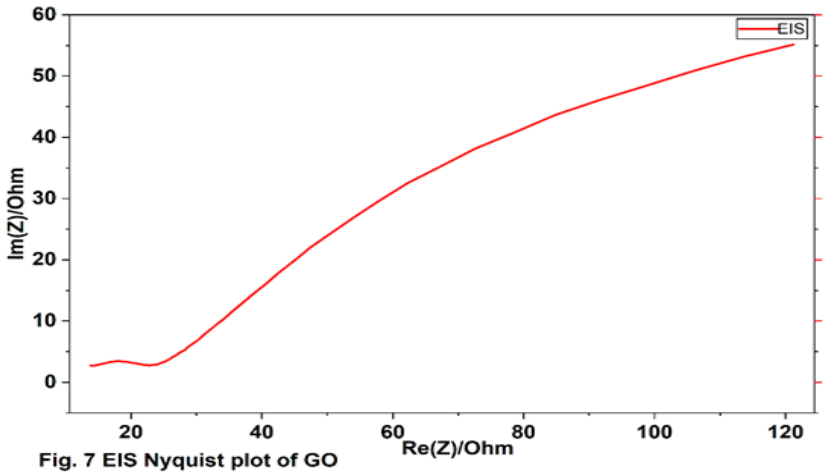

Fig. 7 EIS Nyquist plot of GO

Table 3: Summary Of The Electrochemical Analysis Of The Go

Sample	Mass (g)	C_{sp} (Fg^{-1})	ESR(Ω)	Rct(Ω)	$\Delta E(V)$	$E_d(WhKg^{-1})$	$P_d(KWKg^{-1})$
Go	0.001	21.2	13.8	107.38	1.49	6.54	40.16

Table 3 is the summary of the electrochemical analysis of GO, the value of the specific capacitance is an indication that the material is suitable as a baseline material to be improved via composites, or doping for a higher capacitive performance. From the Nyquist plot (Fig. 7), the equivalent series resistance (ESR) and charge transfer resistance (Rct) were directly extracted. ESR corresponds to the high-frequency intercept of the Nyquist curve with the real axis (Re(Z)), which in this case was measured as 13.82 Ω. Rct is represented by the diameter of the semicircle along the real axis, defined as the difference between the low-frequency and high-frequency intercepts. This means that the electrode shows slightly high ESR (~13.82 Ω) and a very high Rct (~107.38 Ω), indicating low charge transfer at the electrolyte interface as a result of some internal resistance, likely due to oxygen functionalities and defects in GO sheets.

CONCLUSION

In summary, graphene oxide (GO) was successfully synthesized using the improved modified Hummers method. Its morphological and structural characteristics were thoroughly examined. SEM analysis revealed flake-like, irregular layered fragments typical of GO sheets, with a rough and uneven surface texture attributed to exfoliation and oxidation processes. The XRD peak at ~9.2° corresponds to the (001) diffraction plane characteristic of GO due to increased interlayer spacing from oxygen functional groups and water molecules arising from the oxidation of the graphite powder. The FT-IR of the graphene oxide spectrum confirms the presence of oxygen-containing functional groups (hydroxyl, epoxy, carboxyl) that are characteristic of GO. These groups are responsible for GO's hydrophilicity and reactivity, making it useful in composites, membranes, and biomedical applications. The GO gave good electrochemical properties with energy density and power density of $6.54\,Whkg^{-1}$ and $40.16\,KWkg^{-1}$ respectively. However, there is the need to improve on both the ESR and Rct to enhance better performance in energy storage by reducing the O-H functional group and as well as incorporating transition metal to form composites.

REFERENCES

Abakumov, O. O., Bychko, I. B., & Trypolskii, A. I. (2021). Structural Characteristics of Graphene Oxide Reduced by Hydrazine and Hydrogen. Theoretical and Experimental Chemistry, 57, 289–296. https://doi.org/10.1007/s11237-021-09697-z

Abbas, Q., Shinde, P. A., Abdelkareem, M. A., Alami, A. H., Mirzaeian, M., Yadav, A., & Olabi, A. G. (2022, November 04). Graphene Synthesis Techniques and Environmental Applications. Materials, 15, 7804. https://doi.org/10.3390/ma15217804

Ali, A., Chiang, Y. W., & Santos, R. M. (2022). X-ray Diffraction Techniques for Mineral Characterization: A Review for Engineers of the Fundamentals, Applications, and Research Directions. Minerals, 12(2), 205. https://doi.org/10.3390/min12020205

Andre, S. (2019). FTIR spectra of Graphene oxide. Mendeley Data, V1. https://doi.org/10.17632/4j2hxyrcf6.1

AtiafK.Jeryo, & Abbas, Q. A. (2020). Synthesis of Graphene OxideNanoparticlesby Laser Ablation System. raqi Journal of Science, 61(9), 2241-2250. https://doi.org/10.24996/ijs.2020.61.9.11

Aunkor, M. T., Mahbubul, I. M., Saidurb, R., & Metselaar, H. S. (2016). The green reduction of graphene oxide. RSC Advances, 06(33), 27807-27828. https://doi.org/10.1039/C6RA03189G

Baruah, A., Newar, R., Das, S., Kalita, N., Nath, M., Ghosh, P., Narayan., M. (2024). Biomedical applications of graphene-based nanomaterials: recent progress, challenges, and prospects in highly sensitive biosensors. Discover Nano, 19(1), 103. https://doi.org/10.1186/s11671-024-04032-6

Bhuyan, M. S., Uddin, M. N., Islam, M. M., Bipasha, F. A., & Hossain, S. S. (2016, February 09). Synthesis of graphene. International Nano Letters, 06, 65–83. https://doi.org/10.1007/s40089-015-0176-1

Bragg, W. H., & Bragg, W. L. (1913). The reflection of X-rays by crystals. Proceedings of the Royal Society of London. Series A, Containing Papers of a Mathematical and Physical Character, 88(605), 428 - 438. https://doi.org/10.1098/rspa.1913.0040

Brame, J., & Griggs, C. (2016). Surface Area Analysis Using the Brunauer-Emmett-Teller (BET) Method: Scientific Operating Procedure Series: SOP-C. Environmental Consequences of Nanotechnologies.

Brodie, B. C. (1859, May 12). On the Atomic Weight of Graphite. . Philosophical Transactions of the Royal Society of London, 149, 249-259. https://doi.org/10.1098/rstl.1859.0013

Brownson, D. A., Lacombe, A. C., Go´mez-Mingotb, M., & Banks, C. E. (2012). Graphene oxide gives rise to unique and intriguing voltammetry. RSC Advaances, 2, 665 - 668. https://doi.org/10.1039/c1ra00743b

Brunauer, S., Emmett, P. H., & Teller, E. (1938). Adsorption of Gases in Multimolecular Layers. Journal of the American Chemical Society, 60(2), 309-319. https://doi.org/10.1021/ja01269a023

Brusko, V., Khannanov, A., Rakhmatullin, A., & Dimiev, A. M. (2024). Unraveling the infrared spectrum of graphene oxide. Carbon, 119507. https://doi.org/10.1016/j.carbon.2024.119507

Chen, S., Zhu, J., Wu, X., Han, Q., & Wang, X. (2010). ACS NANO, 4(5), 2822–2830. https://doi.org/10.1021/nn901311t

Fagiolari, L., Sampo, M., Lamberti, A., Amici, J., Francia, C., Bodoardo, S., & Bella, F. (2022). Integrated energy conversion and storage devices: Interfacing solar cells, batteries and supercapacitors. Energy Storage Materials, 51(6), 400-434. https://doi.org/10.1016/j.ensm.2022.06.051

Ghafuri, H., keshvari, M., Eshrati, F., Hanifehnejad, P., Emami, A., & Zand, H. R. (2025). Catalytic efficiency of GO-PANI nanocomposite in the synthesis of N-Aryl-1,4-Dihydropyridine and hydroquinoline derivatives. Scientific reports, 15(2791). https://doi.org/10.1038/s41598-024-82907-5

Gharbi, O., Tran, M. T., Tribollet, B., Turmine, M., & Vivier, V. (2020). Revisiting cyclic voltammetry and electrochemical impedance spectroscopy analysis for capacitance measurements. Electrochim Acta, 343, 136109.

Goyat, R., Saharan, Y., Singh, J., Umar, A., & Akbar, S. (2022). Synthesis of Graphene-Based Nanocomposites for Environmental Remediation Applications: A Review. Molecules, 17(19), 6433. https://doi.org/10.3390/molecules27196433

Hansora, D. P., Shimpi, N. G., & Mishra, S. (2015). Graphite to Graphene via Graphene Oxide: An Overview on Synthesis, Properties, and Applications. JOM, 67, 2855–2868. https://doi.org/10.1007/s11837-015-1522-5

Heinze, J. (1984). Cyclic voltammetry—"electrochemical spectroscopy New analytical methods. Angew Chem Int Ed Engl, 23(11), 831–847.

Hossain, M. A., Sheikh, K., Sagar, M. S., Hossain, K. R., X. Y., Bai, C., & Wang, X. (2023). Study on Polymer Intelligent Materials and Actuators Based Graphene. Chemical Review and Letters, 6(4), 461-478. https://doi.org/10.22034/crl.2023.422879.1255

Huang, H., Park, H., & Huang, J. (2022). Self-crosslinking of graphene oxide sheets by dehydration. Chem, 2432–2441. https://doi.org/10.1016/j.chempr.2022.05.016

Huld, F., Mahlen, J., Keller, C., Lai, S., Eleri, O., Koposov, A., & ... Lou, F. (2023). Revealing silicon's delithiation behaviour through empirical analysis of galvanostatic charge–discharge curves. Batteries , 9(5), 251.

Hummers, W. S., & Offeman, R. E. (1958, March 01). Preparation of Graphitic Oxide. Journal of the American Chemical Society, 80(06), 1339. https://doi.org/10.1021/ja01539a017

Jiˇrí ˇcková, A., Jankovský, O., Sofer, Z., & DavidSedmidubský. (2022). Synthesis and Applications of Graphene Oxide. Materials, 15, 920. https://doi.org/10.3390/ma15030920

Krishnamoorthy, K., Veerapandian, M., Yun, K., & Kim, S.-J. (2013). The chemical and structural analysis of graphene oxide with different degrees of oxidation. C A R B ON, 53, 38-49. https://doi.org/10.1016/j.carbon.2012.10.013

Kumar, N., Salehiyan, R., Chauke, V., Botlhoko, O. J., Setshedi, K., Scriba, M., Ray., S. S. (2021, May). Top-down synthesis of graphene: A comprehensive review. FlatChem, 27, 100224. https://doi.org/10.1016/j.flatc.2021.100224

Lee, H. C., Liu, W.-W., Chai, S.-P., Mohamed, A. R., Aziz, A., Khe, C.-S., . . . Hashim, U. (2017). Review of the synthesis, transfer, characterization and growth mechanisms of single and multilayer graphene. RSC Advances, 07, 15644–15693. https://doi.org/10.1039/c7ra00392g

Li, F., Jiang, X., Zhao, J., & Zhang, S. (2015). Graphene oxide: A promising nanomaterial for energy and environmental applications. Nano Energy, 16, 488-515. https://doi.org/10.1016/j.nanoen.2015.07.014

Libber, M., Gariya, N., & Kumar, M. (2025). A comprehensive analysis of supercapacitors with current limitations and emerging trends in research. Journal of Solid State Electrochemistry, 513–527. https://doi.org/10.1007/s10008-024-06107-x

Lim, J. Y., Mubarak, N., Abdullah, E., Nizamuddin, S., Khalid, M., & Inamuddin. (2018, October 25). Recenttrendsinthesynthesisofgraphene andgrapheneoxidebasednanomaterials for removal of heavy metals-Areview. Journal of Industrial and Engineering Chemistry, 66, 29-44. https://doi.org/10.1016/j.jiec.2018.05.028

Liu, W.-W., Chai, S.-P., Mohamed, A. R., & Hashim, U. (2014, July 25). Synthesis And Characterization of Graphene and Carbon Nanotubes: A Review on the Past and Recent Developments. Journal of Industrial and Engineering Chemistry, 20(04), 1171–1185. https://doi.org/10.1016/j.jiec.2013.08.028

Mahdi, F., Javanbakht, M., & Shahrokhian, S. (2024). Facile In-Situ Electrosynthesis of MnO2/RGO Nanocomposite for High Power and Energy Supercapacitors. Journal of Electroanalytical Chemistry, 957, 118099. https://doi.org/10.1016/j.jelechem.2024.118099

Marcano, D. C., Kosynkin, D. V., Berlin, J. M., Sinitskii, A., Sun, Z., Slesarev, A., Tou, J. M. (2010, July 22). Improved Synthesis of Graphene Oxide. ACS NANO, 04(08). https://doi.org/10.1021/nn1006368

Mbayachi, V. B., Ndayiragije, E., Sammani, T., Taj, S., Mbuta, E. R., & khan, A. u. (2021). Graphene synthesis, characterization and its applications: A review. Results in Chemistry, 03, 100163. https://doi.org/10.1016/j.rechem.2021.100163

Mehmood, Z., Shah, S. A., Omer, S., Idrees, R., & Saeed, S. (2024). Scalable synthesis of high-quality, reduced graphene oxide with a large C/O ratio and its dispersion in a chemically modified polyimide matrix for electromagnetic interference shielding applications. RSC Advances, 14, 7641-7654. https://doi.org/10.1039/D4RA00329B

Mujib, S. B., Ribot, F., Gervais, C., & Singh, G. (2021). Self-supporting carbon-rich SiOC ceramic electrodes for lithium-ion batteries and aqueous supercapacitors. RSCAdvances, 11(56), 35440-35454. https://doi.org/10.1039/D1RA05968H

Narayana, M. V., & Jammalamadaka, S. N. (2016). Tuning Optical Properties of Graphene Oxide under Compressive Strain Using Wet Ball Milling Method. Graphene, 73-80. https://doi.org/10.4236/graphene.2016.52008

Nováček, M., Jankovský, O., Luxa, J., Sedmidubský, D., Pumera, M., Fila, V., Sofer, Z. (2017). Tuning of graphene oxide composition by multiple oxidations for carbon dioxide storage and capture of toxic metals. Journal of Materials Chemistry A, 5, 2739-2748. https://doi.org/10.1039/c6ta03631g

Novoselov, K. S., Geim, A. K., Morozov, S. V., Jiang, D., Zhang, Y., Dubonos, S. V., Firsov, A. A. (2004). Electric Field Effect in Atomically Thin Carbon Films. Science, 306, 666-669. https://doi.org/10.1126/science.1102896

Novoselov, K., Geim, A., Morozov, S., Jiang, D., Zhang, Y., Dubonos, S., Firsov, A. (2004). Electric Field Effect in Atomically Thin Carbon Films. Science, 306(5696), 666 669. https://doi.org/10.1126/science.1102896

Pan, G., Wang, L., Song, S., Xu, Z., Fu, D., & Zhang, G. (2018). Preparation of Modified Graphene Oxide Nanomaterials for Water and Wastewater Treatment. IOP Conference Series: Earth and Environmental Science. 170. IOP Publishing. https://doi.org/10.1088/1755-1315/170/3/032074

Park, S., An, J., Potts, J. R., Velamakanni, A., Murali, S., & Ruoff, R. S. (2011, March 11). Hydrazine-reduction of graphite- and graphene oxide. CARBON, 49, 3019–3023. https://doi.org/10.1016/j.carbon.2011.02.071

Patterson, A. L. (1939). The Scherrer Formula for X-Ray Particle Size Determination. Physical Review, 56(10), 978–982. https://doi.org/10.1103/PhysRev.56.978

Polichetti, T., Miglietta, M. L., & Francia, G. D. (2010). Overview on graphene: Properties, fabrication and applications. Chemistry Today, 28(06), 6-9.

Politano, G. G., Burza, S., & Versace, C. (2023). Cyclic Voltammetry and Impedance Measurements of Graphene Oxide Thin Films Dip-Coated on n-Type and p-Type Silicon. Crystals, 13(73). https://doi.org/10.3390/cryst13010073

Pope, C. G. (1997). X-Ray Diffraction and the Bragg Equation. Journal of Chemical Education, 74(1), 129-131. https://doi.org/10.1021/ed074p129

Ray, A., & Saruhan, B. (2021). Application of Ionic Liquids for Batteries and Supercapacitors. Materials, 14(11), 2942. https://doi.org/10.3390/ma14112942

Schlumberger, C., & Thommes, M. (2021). Characterization of Hierarchically Ordered Porous Materials by Physisorption and Mercury Porosimetry—A Tutorial Review. Advanced Materials Interfaces, 8, 2002181. https://doi.org/10.1002/admi.202002181

Shin, D. S., Kim, H. G., Ahn, H. S., Jeong, H. Y., Kim, Y.-J., Odkhuu, D., Kim, B. H. (2017). Distribution of oxygen functional groups of graphene oxide obtained from low-temperature atomic layer deposition of titanium oxide. RS Advances, 7, 13979–13984. https://doi.org/10.1039/c7ra00114b

Sing, K., Everett, D., Haul, R., Moscou, L., Pierotti, R., Rouquérol, J., & Siemieniewska, T. (1985). IUPAC Recommendations 1984: Reporting Physisorption Data for Gas Solid Systems with Special Reference to the Determination of Surface Area and Porosity,. Pure & Applied Chemistry, 57(04), 603 - 619.

Speakman, S. A. (n.d.). Estimating Crystallite Size Using XRD. MIT Center for Materials Science and Engineering. Retrieved from http://prism.mit.edu/xray

Staudenmaier, L. (1899). Verfahren zur darstellung der graphitsäure. Berichte der deutschen chemischen Gesellschaft, 32, 1394–1399. https://doi.org/10.1002/cber.18990320208

Sun, L., Yuan, G., Gao, L., Yang, J., Chhowalla, M., Gharahcheshmeh, M., Liu, Z. (2021). Chemical vapour deposition. . Nature Reviews Methods Primers , 01(05). doi:10.1038/s43586-020-00005-y

Surekha, G., Krishnaiah, K. V., Ravi, N., & Suvarna, R. P. (2020). FTIR, Raman and XRD analysis of graphene oxide films prepared by modified Hummers method. Journal of Physics: Conference Series, 1495 (012012). https://doi.org/10.1088/1742-6596/1495/1/012012

Tene, T., Guevara, M., Valarezo, A., Salguero, O., Arias, F. A., Arias, M., Gomez, C. V. (2021). Drying-Time Study in Graphene Oxide. Nanomaterials, 11, 1035. https://doi.org/10.3390/nano11041035

Thakur, S., & Karak, N. (2012, November). Green reduction of graphene oxide by aqueous phytoextracts. Carbon, 50(14), 5331-5339. https://doi.org/10.1016/j.carbon.2012.07.023

Thakur, S., Badoni, A., Sharma, R., Panda, S., Samriti, Ojha, A., Prakash, J. (2026). Graphene oxide as smart sustainable nanomaterial: a versatile multifunctional material with transformative potential in advanced materials science research. npj Materials Sustainability|, 4(8). https://doi.org/10.1038/s44296-026-00095-x

Thakur, S., Badoni, A., Sharma, R., Panda, S., Samriti, Ojha, A., Prakash, J. (2026). Graphene oxide as smart sustainable nanomaterial: a versatile multifunctional material with transformative potential in advanced materials science research. npj materials sustainability, 4(8). https://doi.org/10.1038/s44296-026-00095-x

Thangaraj, B., Mumtaz, F., Abbas, Y., Anjum, D. H., Solomon, P. R., & Hassan, J. (2023). Synthesis of Graphene Oxide from Sugarcane Dry Leaves by Two-Stage Pyrolysis. Molecules, 28, 3329. https://doi.org/10.3390/molecules28083329

Trikkaliotis, D. G., Christoforidis, A. K., Mitropoulos, A. C., & Kyz, G. Z. (2021). Graphene Oxide Synthesis, Properties and Characterization Techniques: A Comprehensive Review. ChemEngineering 2021, 5(3), 64;, 5(3), 64. https://doi.org/10.3390/chemengineering5030064

Vangari, M., Pryor, T., & Jiang, L. (2013). Supercapacitors: Review of Materials. JOURNAL OF ENERGY ENGINEERING, 139(2), 72-79. https://doi.org/10.1061/(ASCE)EY.1943-7897.0000102

Vessally, E., Rzayev, R. M., Niyazova, A. A., Aggarwal, T., & Rahimova, K. E. (2024). Overview of recent developments in carbon-based nanocomposites for supercapacitor applications. RSC Advances, 14(40141), 40141–40159. https://doi.org/10.1039/d4ra08446b

Williamson, G., & Hall, W. (1953). X-ray line broadening from filed aluminium and wolfram. Acta Metallurgica, ., 1(1), .22–31. https://doi.org/10.1016/0001-6160(53)90006-6

Yazdi, G. R., Iakimov, T., & Yakimova, R. (2016). Epitaxial Graphene on SiC: A Review of Growth and Characterization. Crystals, 6(5), 53. https://doi.org/10.3390/cryst6050053

Ye, R., & Tour, J. M. (2019, December 22). Graphene at Fifteen. ACS Nano, 13(10), 10872–10878. https://doi.org/10.1021/acsnano.9b06778

Yoon, K.-Y., & Dong, G. (2019). Liquid-phase bottom-up synthesis of graphene nanoribbons. Mater. Chem. Front. , 04, 29-45. https://doi.org/10.1039/C9QM00519F

Zhan, M., Xu, M., Lin, W., H. H., & He, C. (2025). Graphene Oxide Research: Current Developments and Future Directions. Nanomaterials, 15, 507. https://doi.org/10.3390/nano15070507

Zhu, L., Ai, Z., Wang, B., Zhang, S., Zou, R., Huang, Y., & Sun, W. (2022). Pseudocapacitive behaviour of Ce modified CoO through a galvanostatic charge–discharge test: distinguishing between surface-control and diffusion-control current. J Phys Chem C, 126(25), 10327–10334.